Biosensors and Bioelectronics 40 (2013) 283–290

Contents lists available at SciVerse ScienceDirect

Biosensors and Bioelectronics

journal homepage: www.elsevier.com/locate/bios

A robust nanoscale biomemory device composed of recombinant azurin on hexagonally packed Au-nano array

Ajay Kumar Yagati [a], Taek Lee [b], Junhong Min [c], Jeong-Woo Choi [a,b,*]

[a] Interdisciplinary Program of Integrated Biotechnology, Sogang University, Seoul 121-742, Korea
[b] Department of Chemical and Biomolecular Engineering, Sogang University, 35 Baekbeom-ro (Sinsu-dong), Mapo-gu, Seoul 121-742, Korea
[c] School of Integrative Engineering, Chung-Ang University, Heukseok-dong, Dongjak-gu, Seoul 156-756, Republic of Korea

ARTICLE INFO

Available online 3 August 2012

Keywords:
Recombinant azurin
Cyclic voltammetry
Electrochemical scanning tunneling microscopy
Nanosphere
Nanoscale biomemory
Nanobiochip

ABSTRACT

We developed a nanoscale memory device consisting of signal-responsive biomaterial, which is capable of switching physical properties (such as electrical/electrochemical, optical, and magnetic) upon application of appropriate electrical signals to perform memory switching. Here, we propose a highly robust surface-confined switch composed of an electroactive cysteine-modified azurin immobilized on an Au hexagonal pattern formed on indium tin oxide (ITO) substrates that can be controlled electrochemically and reversibly converted between its redox states. The memory effect is based on conductance switching, which leads to the occurrence of bistable states and behaves as an extremely robust redox switch in which an electrochemical input is transduced into optical and magnetic outputs under ambient conditions. The fact that this molecular surface switch, operating at very low voltages, can be patterned and addressed locally, and also has good stability and excellent reversibility, makes it a promising platform for nonvolatile memory devices.

1. Introduction

Due to continuously increasing demand for ultimate miniaturization of electronic systems, molecular electronic devices are currently thriving as alternative technologies because of their promising potential in writing, reading, and processing of information at the nanoscale (Waser and Rudiger, 2004). Nanostructures exhibit optical, thermal, electrical, and magnetic properties that differ from bulk materials (Vaseashta and Dimova-Malinovska, 2005). To apply these properties to functional devices, it is often important to control their size, shape, and position on a substrate (Liz-Marzán, 2004). To achieve increasing demand for miniaturization, considerable attention has been paid to develop nanoscale devices by overcoming the technical difficulties that are currently facing the semiconductor industry. Micro-fabrication technologies are reaching fundamental diffraction limits as feature sizes approach 100 nm. Hence, there is a substantial interest in developing nanofabrication techniques to achieve both high resolution and high throughput. Several techniques have been explored with the goal of creating ordered arrays such as: (i) anodized aluminum oxide (Jung et al., 2004), which has drawbacks, such as low throughput and high cost; (ii) interference lithography (Zuppella et al., 2009), which is limited to patterning arrayed features only; (iii) self-assembly of nanoparticles, laser focused atomic deposition (Behringer et al., 1996), which has a major limitation is (a) its slowness; (b) many technologically important materials (Si, Ge, Si_3N_4, several multi-component oxides, certain metals) cannot be deposited in a cost-effective way and (c) being a chemical technique there is always a risk of residues being left from the precursors and (iv) diffusion controlled aggregation and surfaces (Roder et al., 1993), which has limitations, such as diffusion stops when an adaotm hits a stable aggregate and condenses there. Also, it is temperature dependent. Apart form these techniques, nanolithography based on scanning tunneling microscopy (STM) has received considerable attention, (Williams and Gorman, 2007) as it is useful for imaging and can operate at atomic scale (Eigler et al., 1991; Stroscio and Eigler, 1991). However, application of Scanning tunneling microscopy (STM) lithography, like electron beam lithography, has drawback as it is limited by serial processing speeds. Additonally, these techniques utilize complex procedures; thus, novel approaches to parallel nanolithography are being explored. Recently, colloidal or nanosphere lithography which is emerged as an effective and inexpensive method for patterning nanostructures over a large area (Whitney et al., 2004) in which the colloidal nanospheres act as a *mask*. Regular pattern of desired material can be obtained by after deposition and the removal of mask.

Because of high surface-to-volume ratio and tunable electron transport properties due to quantum confinement effect, nanostructures can be used for both efficient transport of electrons and

* Corresponding author at: Department of Chemical and Biomolecular Engineering, Sogang University, 35 Baekbeom-ro (Sinsu-dong), Mapo-gu, Seoul 121-742, Korea. Tel.: +82 2 705 8480; fax: +82 2 3273 0331.
E-mail addresses: jwchoi@sogang.ac.kr, jwchoi@ccs.sogang.ac.kr (J.-W. Choi).

0956-5663/$ - see front matter © 2012 Elsevier B.V. All rights reserved.
http://dx.doi.org/10.1016/j.bios.2012.07.055

optical excitation, and these two factors make them critical to the function and integration of nanoscale devices. In addition, the sizes of biological macromolecules, such as proteins, enzymes, and nucleic acids, are comparable to nanoscale building blocks. Therefore, any interaction between such biomolecules should induce significant changes in the electrical properties of nanostructured biointerfaces. But, one of the major goals of nanoelectronics is to make use of single molecules that function as switches on nanoscale electrode surfaces. This requires developing molecules that can reversibly switch between two conductive states in response to an external voltage/trigger. Azurin possesses two distinct electrochemical states, a reduced and oxidized states that can be reversibly controlled to develop a nanoscale switch. In our previous studies, a protein-based memory was demonstrated using a monolayer of ferredoxin, a redox protein, as an active material and an intrinsic switching mechanism (Yagati et al., 2010). Furthermore, a write-once–read-many times (WORM) type protein-based memory using a redox recombinant protein has been demonstrated (Yagati et al., 2009a). Multi-bit protein-based memory to store multiple bits electrochemically at a time and its read-out mechanism has been proposed (Yagati et al., 2009b). Also, digital memory device based on virus conjugated with nanoparticles where virus was used as a template for ordering quantum dots (Tseng et al., 2006). Further, a protein-based associative processors and volumetric memory was proposed by Birge et al., 1999. However, a method to *read* the electrochemically stored charge with optical and magnetic properties of protein molecules at the nanoscale level for realizing a memory device has not been reported yet.

Blue copper azurin (about 14.6 kDa), the protein of interest in the present study, is responsible for electron transfer in the respiratory system of several bacteria. We introduced cysteine residue into *Pseudomonas aeruginosa* azurin to improve the uniformity of the protein monolayer on the gold surface because a wild-type form of the azurin was irregularly adsorbed to the gold surface via its exposed disulfide moiety (Cys3–Cys26) (Rinaldi et al., 2002). Since azurin has copper as a key element in the electron transfer mechanisms, so this can be used as an electron acceptor in the development of molecular electronic device by mimicking biological mechanism.

Here we report, a protein based memory device, in which the recombinant protein is self assembled on Au patterned indium tin oxide (ITO) coated glass plate without the use of any additional linkers. The morphological and current measurements of azurin molecules were observed by using electrochemical scanning probe microscopy with in-situ cyclic voltammetry experiments. Current measurements were obtained by applying redox potentials to the Az/Au-ITO electrode to ensure proper memory device operation. Apart from that, clear memory device switchings for charge *storage* and *erase* functions were observed with optical and magnetic detection methods. Further, variations in the conductivity of Au thinfilm with an Au nanopattern on an ITO electrode were compared. The device reproducibility and revisbiliy was also examined with application of continuos *write* and *erase* cycles.

2. Materials and Methods

2.1. Chemicals and reagents

Polystyrene particles (0.46 μm, 1% w/w) were purchased from Thermo Scientific (Rockford, IL, USA) and were centrifuged to obtain 10% w/w. Polyoxyethylene (20) sorbitan monolaurate was obtained from Sigma-Aldrich. 4-(2-Hydroxyethyl) piperazine-1-ethanesulfonic acid (HEPES), buffer solution (10 mM, pH 7.0) was used in electrochemical experiments. All other solutions were prepared with water (18 MΩ cm) purified using by a Milli-Q system (Millipore, Bedford, MA, USA).

2.2. Electrode cleaning procedure

ITO-coated glass substrates with dimensions $10 \times 10\ mm^2$ with a thickness of 400 nm were cleaned ultrasonically in successive solutions of Triton X-100/water (1:5, v/v), water and ethanol for at least 40 min each. The substrates were then treated in an oxidizing bath of NH_4OH: H_2O_2: H_2O (1:1:5) at 80 °C for 1 h to remove particulate contaminants and then washed thoroughly with DI water, and dried in N_2 stream.

2.3. Fabrication of Au hexagonal nanopattern on ITO surface

The nanosphere masks were formed by spin-coating polystyrene particles on cleaned ITO substrates using nanosphere lithography technique (Winzer et al., 1996). Particles of 0.46 μm were spin-coated at a speed of 2000 rpm for 20 s. The physical dimensions of the substrate were chosen to be $10 \times 10\ mm^2$, and the entire surface was spin-coated with nano-spheres. The nanospheres of 10 wt% dispersed in water were further diluted in Triton X-100/methanol (1:400 by volume) before spin-coating. The dilution factors for single-layer masks were ca. 1:1 (by volume) for the 460 nm particles. A surfactant was used to assist the solutions to wet the substrate. Double-layer masks were self-assembled by increasing the nanosphere concentration and dilution factors in the spin-coating solution to optimize double layer surface coverage. Thin films of Au were deposited through vacuum evaporation over the coated substrates. To obtain regular pattern, the polystyrene spheres were lifted off of from the ITO substrate by dissolution in methylene chloride (CH_2Cl_2) with the aid of sonication for 1–2 min as shown in Fig. 1.

2.4. Preparation of recombinant azurin and immobilization on Au nanopattern

Azurin was recombined with cysteine residues by site-directed mutagenesis (Lee et al., 2010; Choi et al., 2009). Cysteine modified azurin was immobilized on the patterned Au array by the strong affinity between the thiol of cysteine and Au. 20 μl of prepared recombinant azurin (0.1 mg/ml) was dropped on the Au pattern over 3 h and then treated with 0.05% solution of polysorbate20 for 2 h to remove any excess or unbound molecules on the Au triangles. Finally the azurin immobilized Au pattern was cleaned with deionized water and dried under nitrogen stream (Lee et al., 2011).

2.5. Measurements on Au hexagonal nanopattern

The surface topography of each fabrication step was investigated by Scanning electron microscopy (SEM) measurements using a JEOL JSM-7500F operating at a voltage of 15 kV having magnification 25x to 1,000,000x and resolution imaging: 1.4 nm at 1 kV, 1.0 nm at 15 kV.

The electrochemical experiments were performed on Az/Au-ITO surface by using Multimodal Nanoscope III from Veeco Instruments (Plainview, NY, USA) with an electrochemical module (EC-STM) (Digital Instruments). The in-situ cyclic voltammetry was performed using EC-STM bipotentiostat module. A Pt wire as counter and Ag electrode served as quasi-references for the EC-STM experiments. Pt/Ir tips (14 mm) were purchased from Veeco Instruments and were insulated using apiezon wax polish to measure the tunneling current and effectively blocking the leakage/background currents. Images were scanned at $E_{bias} = 100$ mV, $I_{tip} = 4$ nA with a rate of 1 Hz.

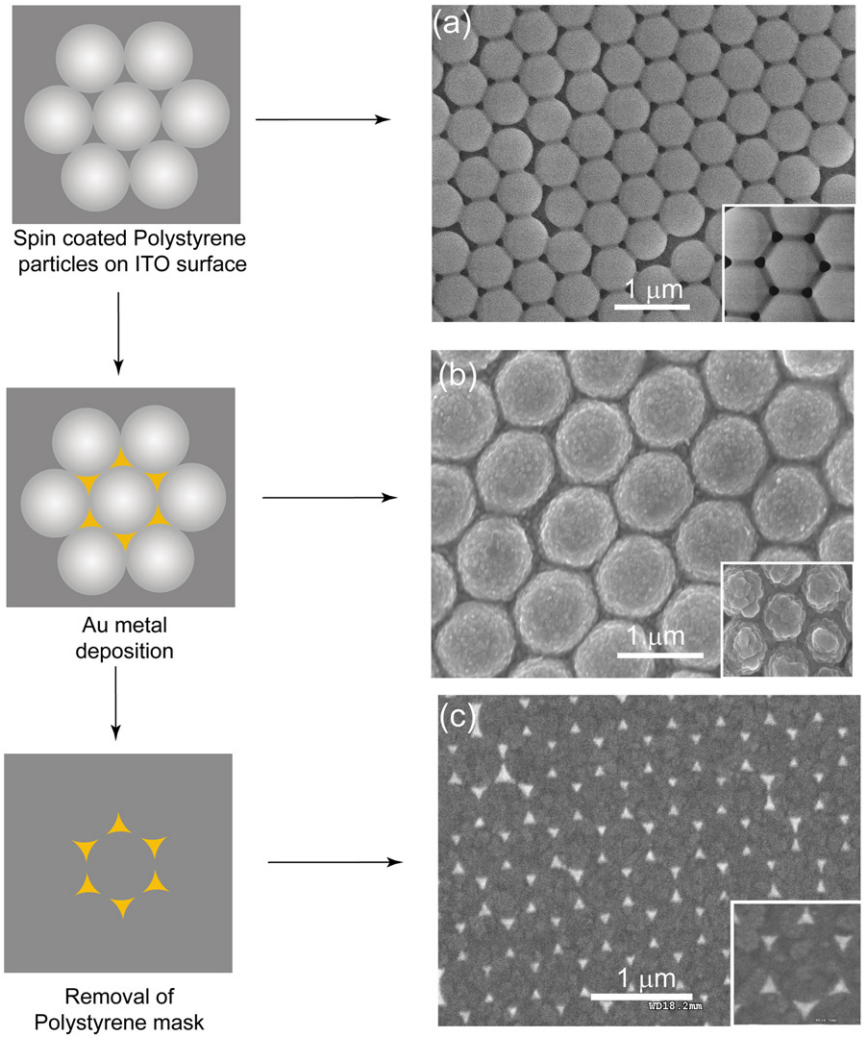

Fig. 1. (a) Schematic diagram for the fabrication of Au nanopattern on ITO substrate by nanosphere lithography (NSL) and corresponding SEM images at each step of the formation of a hexagonal nano-pattern on the ITO substrate.

Optical measurements were conducted using a JASCO-V-660 spectrophotometer. The dimensions of the substrates were 20 mm^2 with bare ITO as a reference sample. Electron spin resonance (ESR) spectra were measured using a JEOL RE-2X spectrometer equipped with the ES-IPRITS/TE data system software on a PC. Precautions to avoid undesirable spectral distortions and line broadenings, such as those arising from microwave power saturation and magnetic field over modulation, were also considered for improved sensitivity. For the conductivity comparison measurements, the resistance of the deposited bulk Au layer with the Au pattern on the ITO substrate was measured using a Keithley 2420 3 A source meter (Solon, OH, USA) with four point probes.

3. Results and discussion

3.1. Morphology of the Au-hexagonal nanopattern

The morphology of Au nanopattern on ITO was examined with SEM analyses as shown in Fig. 1. SEM image of 460 nm deposited particles on the ITO surface, in which the particles clearly showed a monolayer of spheres forming an ordered close-packed hexagonal array having voids between the spheres shown in Fig. 1a. After thermal evaporation of Au Fig. 1b, the polystyrene particles were chemically removed and the resultant pattern is shown in Fig. 1c. The deposited metal reached the substrate through the voids in the close packed mask, which resulted in a honeycomb array gold nanopattern after removing the mask. The resulting pattern shows that the honeycomb pattern of Au-dots (of quasi triangular shape) was well formed on the ITO substrate without any artifacts. The analysis revealed that the particle size was 436 nm with height about 110 nm.

However, few dots were joined together to form Au nanowires, which may have been due to (a) small portion of polystyrene particles that were not uniform. When slightly different sized particles are introduced in the monolayer, the orderly structural area is disturbed to increase the voids between the spheres. When Au was deposited, Au nanowire formed in these voids; (b) the thickness of the Au dots was greater than the desired thickness during the deposition process due to a non-uniform deposition rate, which leads to the formation of nanowires.

If the formed area is considered as an equilateral triangle, then one of the side lengths could be determined using the following equation:

$$a_{\Delta} = \left(4 - \frac{2}{\sqrt{3}}\pi\right)^{1/2} R = 0.61R \quad (1)$$

where a_{Δ} is the side length of the triangle.

From Eq. (1), it can be seen that Au triangle with a side length of 140.3 nm was formed when the radius of the microsphere is

230 nm, which is in agreement with the results obtained by the SEM and AFM. Here, a particle size of 460 nm was selected to provide enough space between two Au nano-triangles, because if two Az/Au-ITO triangles were close enough, the electrochemical measurements will ultimately change thereby influencing device performance (Fig. S1). Furthermore, the hexagonal patterns obtained from single and double layer (DL) masks were compared as shown in Fig. S2, and the AFM section analysis can be seen in Fig. S3. The pattern obtained from a DL mask was slightly different from that obtained with a single layer (SL) mask; the DL mask forms a circular pattern, whereas the SL mask leads to a quasi triangular pattern as shown in Fig. S2(c and f).

3.2. *Confirmation of protein immobilization: electrochemical scanning tunneling microscopy (ECSTM) with in-situ cyclic voltammetry*

Electrochemical experiments on Az/Au-ITO were conducted by ECSTM with in-situ cyclic voltammetry. Experiments were carried out in 10 mM HEPES buffer solution, where the Az/Au-ITO substrate acts as working electrode (vs. Ag/Ag^{+}) as shown in Fig. 2a (i). The biomemory mechanism is shown in Fig. 2a (ii). The cyclic voltammogram of bare Au nanopattern did not reveal any redox peaks; however, the CV for azurin on the Au nanopattern clearly depicted the peak reduction at −0.07 V and an oxidation peak at 0.36 V, respectively, at a scan rate of 50 mV/s, which corresponded to the redox process of the $Cu^{2+/1+}$ center in azurin, as shown in Fig. 2b (i and ii). The formal reduction potential ($E_{1/2}$), calculated as $E_{1/2} = (E_{pc} + E_{pa})/2$, was 0.14 V, which was slightly shifted due to the reference electrode used in the present system. CV's obtained for both bare Au and Az/Au with Ag/AgCl electrode are also shown, where bare Au does not reveal any peaks however Az/Au shows broad peaks corresponds to oxidation and reduction of Azurin and with its currents increased linearly with increase in scan rate, which is characteristic of surface-confined electroactive species Fig. 3(b and d). These two redox states of azurin were used for charge storage and erase functions to develop a molecular switch for the ON and OFF function. The stability of the two redox states was analyzed by applying many consecutive voltage cycles, which resulted in completely identical voltammograms without any loss of current intensity. From these results, it was estimated that a reversible and stable switch can be realized with an Az/Au-ITO electrode a. Furthermore, an estimate of surface coverage of the protein molecules on the Au nano-triangle was obtained using the following equation:

$$I_p = \left(n^2F^2/4RT\right)\Gamma A\upsilon_{ramp} \quad (2)$$

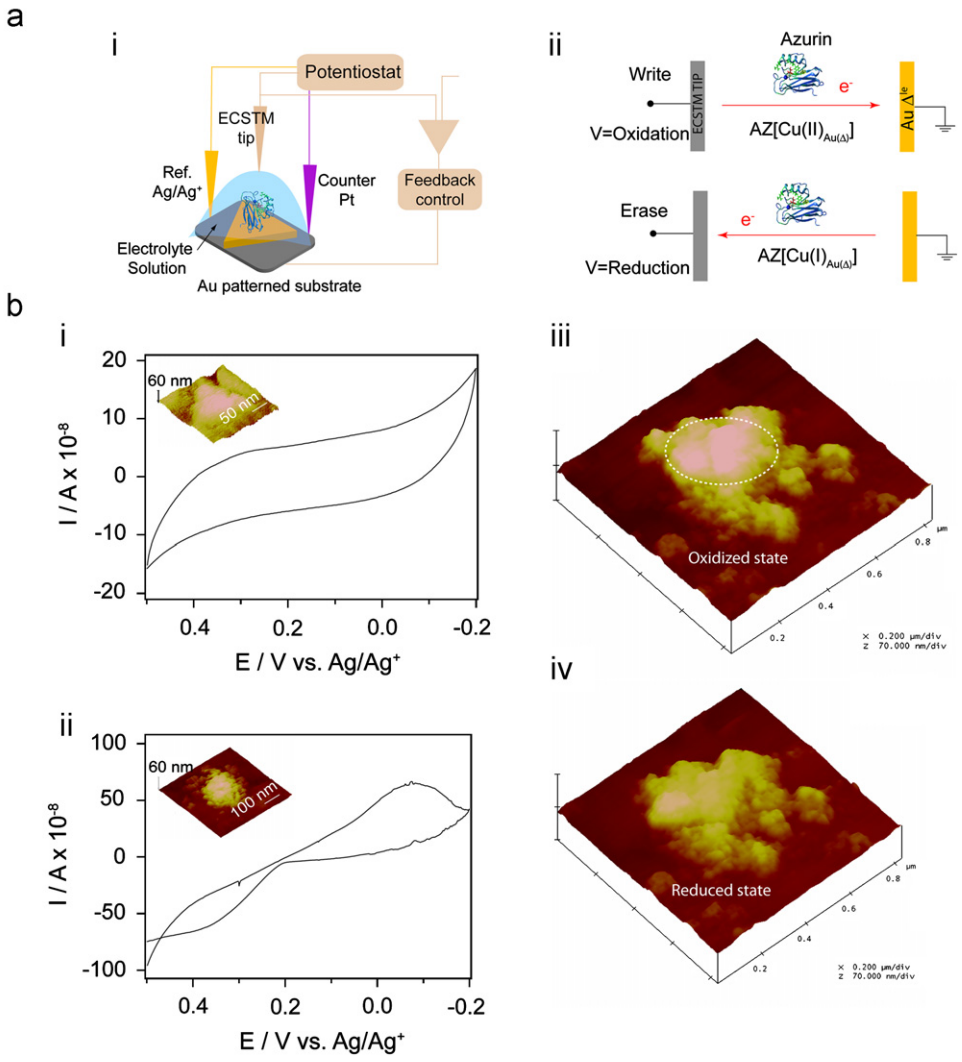

Fig. 2. (a) Schematic diagrams shows (i) Az/Au triangle with ECSTM set-up and (ii) electron transfer mechanism in Az/Au nano-triangle during oxidation and reduction potentials. (b) CV's for (i) bare and (ii) Az/Au/ITO in 10 mM buffer solution pH 7.0 at a scan rate of 50 mV/s. *inset* shows ECSTM images of (i) bare Au and (ii) Az/Au/ITO surface. Potential dependent ECSTM images of Az/Au/ITO for (iii) oxidation (0.36 V) and (iv) reduction potentials (−0.07 V) respectively.

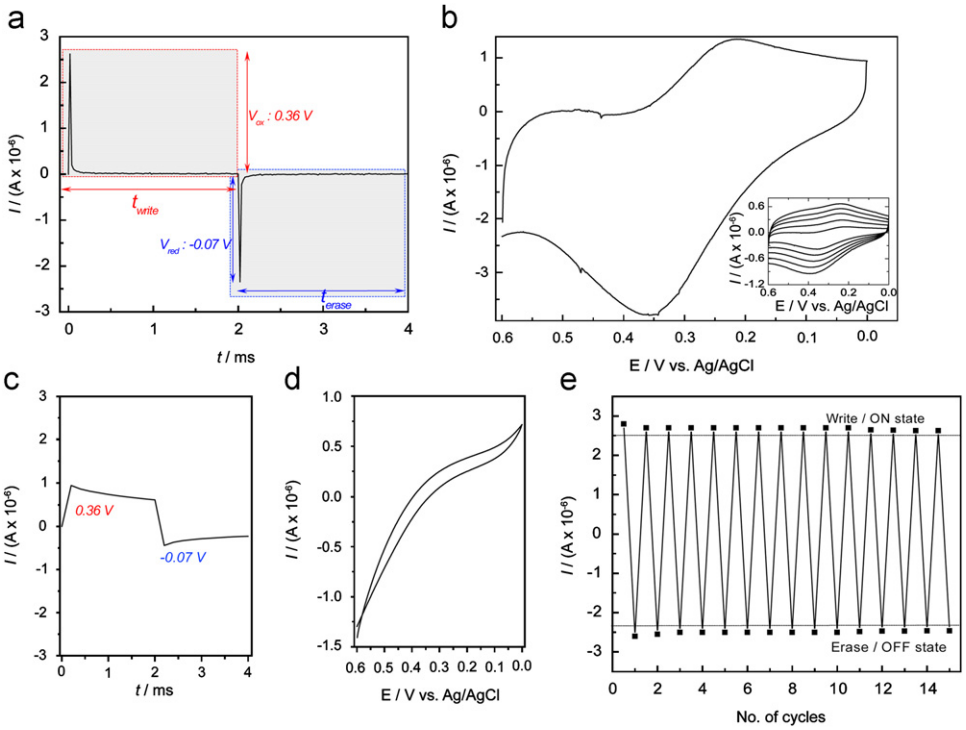

Fig. 3. (a) Faradaic switching currents obtained for charge write and erase (I_{write} and I_{erase}) on applying both oxidation and reduction voltages for a duration (t_{write}) of 2 ms, (b and d) CV's obtained for Az/Au and bare Au surface in 10 mM HEPES buffer pH 7.0 at a scan rate of 0.1 Vs^{-1} *inset* shows the effect of scan rate on Az/Au surface and (c) currents obtained on the bare Au pattern upon the application of both oxidation and reduction voltages for duration of 2 ms. (e) Charge storage and erase currents observed from the device with a 2 ms pulse for applied voltages of 0.36 V and −0.07 V for 15 continuous cycles.

where I_p is peak current (anodic or cathodic), v_{ramp} is voltage ramp rate, Γ is surface coverage, n is number of electrons, A is the surface area, F is Faraday constant, R is gas constant, and T temperature. Using this equation, the surface coverage on a single Au nano-triangle was estimated to be 1.526×10^8 molecules/nm^2. The surface morphology of the bare and protein immobilized single Au nano-triangle was investigated by ECSTM as shown in the *inset* of Fig. 2b (i and ii). As it can be seen, well adsorbed protein molecules were formed on the Au nano-triangle and could be distinguished from its bare counterparts.

3.3. Potential dependent charge storage in the azurin monolayer for molecular memory operation

EC-STM imaging was performed in constant-current mode on the azurin adsorbed on the Au nanotriangle. A set of images of the same sample area was obtained at constant bias while varying the potential. It was observed from the imaging that there was a variation in the conductance of the redox molecules upon varying the potential which was reflected in a difference in apparent height with respect to the background. Fig. 2b (iii and iv) shows the images for the applied potential of 0.36 and −0.07 V respectively for a bias voltage of 100 mV for oxidation and reduction states of azurin moelcules. It wsa assumed that at $E_{bias}=0$ V, the redox state of azurin is vacant with energy higher than the fermi energy of the substrate and tip. When a negative bias was applied to the substrate and the tip was kept at the positive potential, the vacant state energy and fermi energy of the substrate were matched, allowing electrons to be transferred from the substrate to the biomolecule, which lowers the thermal activation allowing the biomolecule to transfer the electron to the tip.

We assumed that from the images that there were two conductive states for charge storage. A brighter spot emerged, which was interpreted as a small island of oxidized azurin molecules containing a Cu center. When a voltage of 0.36 E_{ox} was applied, an electron tunnel formed adsorbed azurin molecules on the Au substrate, and lead to a storage of positive charges in the azurin molecules. In contrast, when a voltage of −0.07 E_{red} was applied, the electrons were transferred back to azurin molecules and the stored charge was erased, which was performed to erase the stored charge. In this case, the brighter spot on the Au triangle disappeared, which confirmed that the oxidized azurin molecules were now reduced.

The bright spots on the Au nanotriangles, which contained azurin, were attributed to electron tunneling enhancement due to the presence of the copper active site. These morphological changes appeared to be strongly dependent on the redox potentials. This behavior is consistent with the resonant nature of the current measured in the STM experiments of the Au adsorbed azurin molecules.

3.4. Electrochemical switching of the protein-based memory device

Chronoamperometric measurements were obtained on Az/Au and on a bare Au pattern as working electrode. Currents were recorded by applying oxidation (0.36 V vs. Ag/Ag^+) and reduction (−0.07 V vs. Ag/Ag^+) potentials in 10 mM HEPES buffer solution as shown in Fig. 3(a and c). Sharp current transitions were observed for both the oxidation and reduction potentials on the Az/Au pattern indicating that the device can be switched ON and OFF for charge storage. However, the bare pattern does not show any faradaic currents rather it shows a pulsed waveform similar to the applied voltages which behaves as a pure conductor and cannot store any charge. Additionally, we observed that the reducing current produced the same magnitude of oxidation current in which we assumed that the oxidized azurin molecules were completely reduced. The switch response to a sequence for *write* and *erase* pulses were examined to further demonstrate the potential of the

system to develop a nonvolatile memory device. Short 2 ms *write* (0.36 V) and *erase* (−0.07 V) pulses were applied, and the readings were observed for 15 cycles. As shown in Fig. 3e both switch states were completely stable and reversible. The redox potentials were continuously applied to switch ON and OFF to estimate device stability, which we observed based on the stable redox peaks by CV. The redox properties were maintained for up to 10^3 cycles with little change in peak currents. In addition, the switching robustness at fast-voltage pulses for *write* and *erase* sequences in the range of 10^{-6} s did not show degraded current values. Based on this, the present device showed good endurance for charge storage without loss of any magnitude in the faradaic current.

3.5. Spectroelectrochemical properties of the protein-based memory device

To develop a new read-out mechanism for the memory function, we elucidate the redox processes of Az/Au-ITO substrates and characterized the transient species by localized surface plasmon resonance (LSPR) spectroscopy on application of redox potentials. Surface plasmons are unevenly distributed around nonspherical metallic particles and nanostructures which apparently results in shape-dependent LSPR absorption spectra (Sau et al., 2010). In such cases, the plasmon resonance splits into low- and high-energy absorption bands. The high-energy, or transverse absorption band, corresponds to the electron oscillations perpendicular to the major axis; whereas the low-energy, or longitudinal, absorption band, results from oscillation of electrons along the major axis. Triangular patterns exhibit multiple plasmon resonance, a longitudinal (bulk) plasmon mode and a very large localized enhancement at the sharp tips (Hao et al., 2004). The wavelength corresponding to the extinction maximum of the LSPR (λ_{max}) is also strongly dependent on the dielectric properties of the medium. Fig. 4a–c shows the absorption peak of the Au pattern at a λ_{max} of 550 nm along with LSPR spectroscopy of the azurin oxidized and reduced forms on the Au patterned ITO substrate. By using the Au pattern ITO as a reference electrode, it was observed that an intense peak (λ_{max}) appeared at 621 nm upon applying a voltage of E=0.36 V. Additionally, applying E=−0.07 V resulted in an intense peak (λ_{max}) at 638 nm and a weaker peak at 510 nm. These peaks were due to the ligand-to-metal-charge transfer transition ($S(\mathrm{Cys}-\pi)\rightarrow \mathrm{Cu(II)}d_{x^2-y^2}$) involving the copper atom of the active site and one of the five metal ligands (specifically, Cys 112) (Solomon et al., 1980), which has a band gap energy of 1.98 eV with the ($S(\mathrm{Cys}-\sigma)\rightarrow \mathrm{Cu(II)}d_{x^2-y^2}$) transition (Han et al., 1993), respectively. All these spectral changes are a clear indication of the transformation of Az and its redox states, and the process was reversible.

Groeneveld and Canters (1985) disclosed that reduced azurin has diamagnetic behavior and oxidized azurin behaves as paramagnetic. Hence, magnetic output can also be used to perform the molecular switch for read-out mechanism of the switch. Thus, we measured ESR on the oxidized and reduced forms of azurin as shown in Fig. 5. Fig. 5a shows the signal at g=2.15(at 313.6) and g=4.11(at 163.87) for the oxidized form of azurin, whereas the reduced form (Fig. 5b) released signals at g=2.14 (at 313.6), g=4.09 (at 164.48), and g=1.97 (at 340.9) showing a hyperfine structure for reduced azurin, which is invisible in the oxidized form. Only the signal at g=1.97 (at 340.9) could be detected for the reduced form of azurin; hence, it was estimated that magnetic output can also be used for reading the state of the molecular switch.

Based on these findings, azurin on a hexagonal nanopattern can be used as a nanoscale switch on binary logic circuits. The applied electrochemical voltage can be considered the input; when 0.36 V was applied, the azurin turned to its oxidized form (Input 1) and when −0.07 V was applied the azurin turned back to the reduced form (Input 0). Four output mechanisms can be detected from these inputs: (a) an absorption peak at 621 nm (b) an absorption peak at 638 nm (c) the ESR signal, and the (d) chronoamperometric signal. So, a binary logic gate can be realized from these four outputs.

Both bulk Au and its pattern on ITO surfaces were analyzed by UV–vis diffuse reflectance spectroscopy to further investigate conductivity variations at the nanoscale level. Fig. 6a shows the reflectance spectra of an Au nanopattern on ITO compared with the bulk Au layer on the ITO surface. The spectrum for bulk Au showed an absorbance peak at about 450 nm, which was clear for Au; however, the Au nanopattern also contained an absorbance peak at 550 nm. This broad peak at 550 nm is typical for plasmon absorption of gold nano-clusters (Link and El Sayed, 1999). Using four-probe method the electronic properties of the Au thin film and the Au nanopattern on ITO were compared. In all samples, the thickness of the Au film was 50 nm, which was created by sputtering on SiO_2 and/or ITO substrate with substrate dimensions of 10×10 mm^2. Conductivity was measured when a sweeping current of $\pm$100 μA was applied. Considering the geometrical correction factor, the electrical conductivity of the film was calculated using the following equation (Pham et al., 2011):

$$\sigma = \left(\frac{\ln 2}{2\pi t R}\right) \tag{3}$$

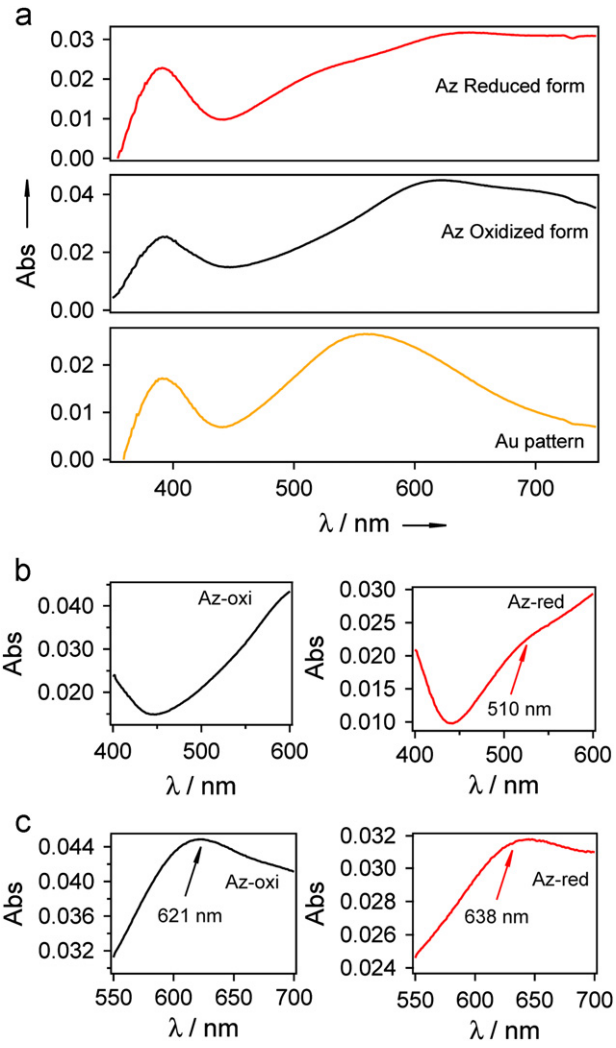

Fig. 4. (a) Absorption spectra of the Au nanopattern on ITO, Az/Au-ITO (both oxidized and reduced forms), (b and c) zoomed images represents the spectra of oxidized (E=0.36 V) and reduced (E=−0.07 V) forms of azurin on the Au-ITO substrate.

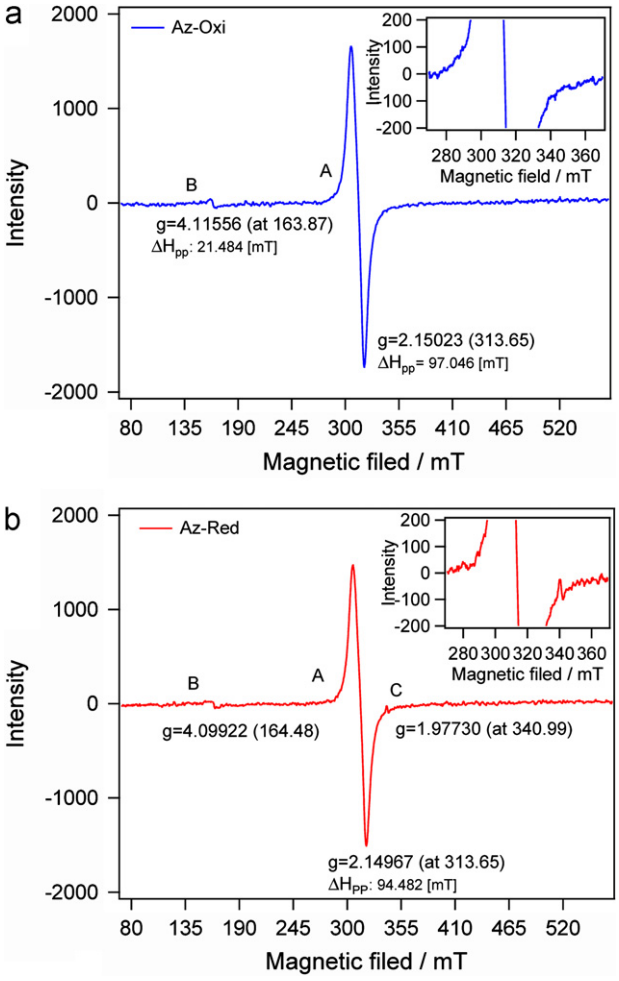

Fig. 5. X-band EPR spectrum of recombinant azurin for the (a) oxidized and (b) reduced states, *inset* shows the zoomed portion of each figure. Instrument settings: microwave frequency, 9.43 GHz; microwave power, 1.00 mW; modulation amplitude, 2 G, modulation frequency, 100 kHz.

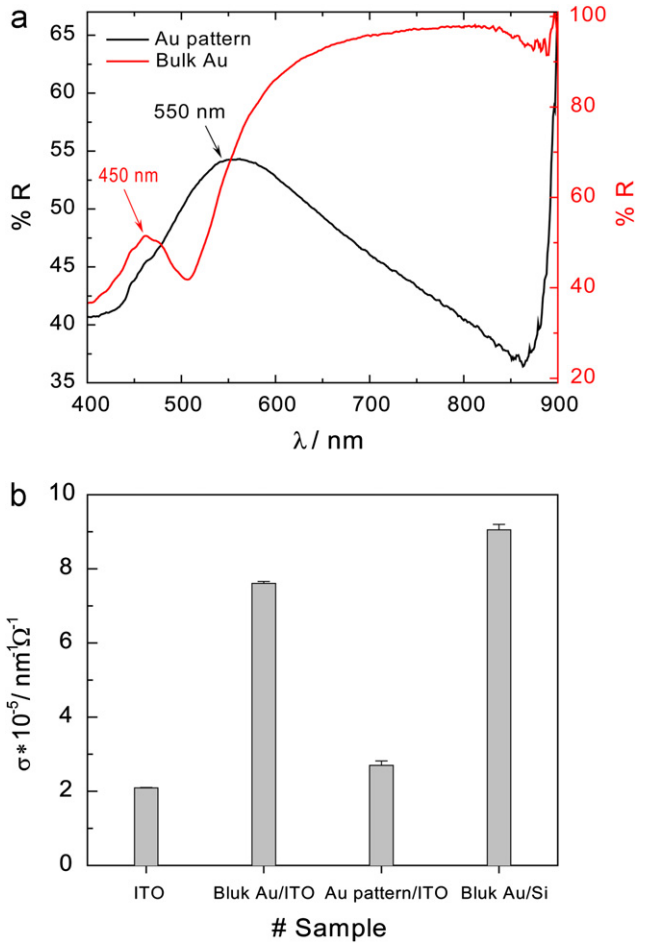

Fig. 6. (a) Diffuse reflectance spectra of bulk and Au array on the ITO substrate and (b) conductivity measurements by four-probe instrument on Au film deposited on different samples.

where, σ is specific conductivity ($S\ nm^{-1}$), t is the thickness (nm) of the deposited gold layer on ITO, and R is the resistance of the film (Ω).

The obtained conductance values for different substrates using Au-deposited thin films are presented in Fig. 6b. In these experiments, the conductivity of bulk Au was greater than that of the Au pattern. The low conductivity value of Au nanopattern may be due to the finite area of contact, which was sufficiently small. In addition, the tips must be positioned above only the pattern of the sample to guarantee a successful measurement of specific resistivity. We assumed that proper positioning of the electrode will lead to high conductivity values as the resistance of the pattern was obviously low compared with that of the bulk Au thin film. Overall, it was assumed that the Au nanopattern ITO possessed more conductivity than that of the bulk materials.

4. Conclusions

In summary, the self-assembled azurin Au nanopattern on ITO was investigated for developing a nanoscale memory device. Based on the electrochemical nature of the protein, it was reversibly converted between its redox states (oxidized and reduced forms) for memory switching operations. Additionally, the optical and magnetic responses can be used as a readout mechanism. Because the azurin was immobilized on an Au pattern, it can be addressed locally, operates at very low voltages with its stability, robustness, and reversibility, making the system a very promising memory device. The proposed approach will directly impact the implementation of recent advances in biotechnology such as Biocomputing systems which uses biomolecules, such as DNA/proteins, to perform computational calculations involving storing, retrieving, and processing data.

Acknowledgments

This study was supported by The Nano/Bio Science and Technology Program (M10536090001-05N3609-00110) of the Ministry of Education, Science, and Technology (MEST), by the National Research Foundation of Korea (NRF) grant funded by the Korea government (MEST) (2012-0000163), and by the Ministry of Knowledge Economy (MKE) and Korea Institute for Advancement in Technology (KIAT) through the Workforce Development Program in Strategic Technology

Appendix A. Supporting information

Supplementary data associated with this article can be found in the online version at http://dx.doi.org/10.1016/j.bios.2012.07.055.

References

Behringer, R.E., Natarajan, V., Timp, G., 1996. Applied Physics Letters 68, 1034–1036.

Birge, R.R., Gillespie, N.B., Izaguirre, E.W., Kusnetzow, A., Lawrence, A.F., Singh, D., Song, Q.W., Schmidt, E., Stuart, J.A., Seetharaman, S., Wise, K.J., 1999. Journal of Physical Chemistry B 103, 10746–10766.

Choi, J.-W., Kim, J.S., Kim, S.-U., Min, J., 2009. Biochip Journal 3, 157–163.

Eigler, D.M., Lutz, C.P., Rudge, W.E., 1991. Nature 352, 600–603.

Groeneveld, C.M., Canters, G.W., 1985. European Journal of Biochemistry 153, 559–564.

Han, J., Loehr, T.M., Lu, Y., Valentine, J.S., Averill, B.A., Sanders-Loehr, J., 1993. Journal of the American Chemical Society 115, 4256–4263.

Hao, E., Bailey, R.C., Schatz, G.C., Hupp, J.T., Li, S., 2004. Nano Letters 4, 327–330.

Jung, M., Kim, H.G., Lee, J.K., Joo, O.S., Mho, S.I., 2004. Electrochimica Acta 50, 857–862.

Lee, T., Kim, S.-U., Min, J., Choi, J.-W., 2010. Advanced Materials 22, 510–514.

Lee, T., Min, J., Kim, S.-U., Choi, J.-W., 2011. Biomaterials 32, 3815–3821.

Link, S., El Sayed, M.A., 1999. Journal of Physical Chemistry B 103, 8410–8426.

Liz-Marzán, L.M., 2004. Materials Today 7, 26–31.

Pham, L.Q., Sohn, J.H., Park, J.H., Kang, H.S., Lee, B.C., Kang, Y.S., 2011. Radiation Physics and Chemistry 80, 638–642.

Roder, H., Hahn, E., Brune, H., Bucher, J.P., Kern, K., 1993. Nature 366, 141–143.

Rinaldi, R., Biasco, A., Maruccio, G., Cingolani, R., Alliata, D., Andolfi, L., Facci, P., De Rienzo, F., Di Felice, R., Molinari, E., 2002. Advanced Materials 14, 1453–1457.

Sau, T.K., Rogach, A.L., Jackel, F., Klar, T.A., Feldmann, J., 2010. Advanced Materials 22, 1805–1825.

Solomon, E.I., Hare, J.W., Dooley, D.M., Dawson, J.H., Stephens, P.J., Gray, H.B., 1980. Journal of the American Chemical Society 102, 168–178.

Stroscio, J.A., Eigler, D.M., 1991. Science 254, 1319–1326.

Tseng, R.J., Tsai, C., Ma., L., Ouyang, J., Ozkan, C.S., Yang, Y, 2006. Nature Nanotechnology 1, 72–77.

Vaseashta, A., Dimova-Malinovska, D., 2005. Science and Technology of Advanced Materials 6, 312–318.

Waser, R., Rudiger, A., 2004. Nature Materials 3, 81–82.

Whitney, A.V., Myers, B.D., Van Duyne, R.P., 2004. Nano Letters 4, 1507–1511.

Williams, J.A., Gorman, C.B., 2007. Langmuir 23, 3103–3105.

Winzer, M., Kleiber, M., Dix, N., Wiesendanger, R., 1996. Applied Physics A 63, 617–619.

Yagati, A.K., Kim, S.-U., Min, J., Choi, J.-W., 2009a. Biosensors and Bioelectronics 24, 1503–1507.

Yagati, A.K., Kim, S.-U., Min, J., Choi, J.-W., 2009b. Electrochemistry Communications 11, 854–858.

Yagati, A.K., Kim, S.-U., Min, J., Choi, J.-W., 2010. Journal of Nanoscience and Nanotechnology 10, 3220–3223.

Zuppella, P., Luciani, D., Tucceri, P., Marco, P.D., Gaudieri, A., Kaiser, J., Ottaviano, L., Santucci, S., Reale, A., 2009. Nanotechnology 20, 115303.